Materials Express

2158-5849/2021/11/732/008
doi:10.1166/mex.2021.1942
www.aspbs.com/mex

Article

Macromechanics, microstructure and particle contact model of artificially cemented laterite

Yong Wang[1], Zhen-Zhong Cao[1], Yong Niu[1], Hai-Bo Lyu[1,2,*], and Yuan Chai[3]

[1]*College of Earth Sciences, Guilin University of Technology, Guilin 541004, China*
[2]*College of Architecture and Electrical Engineering, Hezhou University, Hezhou 542899, China*
[3]*College of Civil Engineering and Architecture, Guangxi University, Nanning 530004, China*

ABSTRACT

In this paper, the research is based on iron hydroxide colloids that combine loose kaolin clay media to form artificial laterite samples. A method and device for the preparation of colloids have been developed. The compressive strength test method is used to explore the regularity and mechanism of free iron oxides which in the process of the formation and strength increase of laterite structure. X-ray diffraction (XRD), scanning electron microscopy (SEM), and nuclear magnetic resonance (NMR) were used to study the mineral composition of the laterite, the cementation of microscopic aggregates of the particles, and the changes in the internal porosity of the laterite. The results show that the free iron oxide can improve the macro-mechanical properties of laterite. The iron morphology has a tendency to change from colloid to hematite and goethite. It is found that the free iron oxide aggregated in the space or on the surface of clay particles. Distribution; gel particles were found to fill the pores of laterite particles or aggregates by nuclear magnetic resonance experiments, indicating that the changes in the mechanical strength of laterite are mainly due to the content of free iron oxide, the formation of free iron oxide, the connection of cementing iron and the distribution of iron. Based on the SEM results, a contact model of laterite particles that can reflect the macro-mechanical failure behavior of soil samples is established.

Keywords: Artificial Laterite, Iron Hydroxide Colloid, Cementation Action, Sensitivity.

1. INTRODUCTION

The major areas of laterite in the world are located in the humid temperate regions between 35 degrees N and 35 degrees S [1–3]. Subtropical climate, which is a humid and heat environment, makes the engineering characteristics of laterite very sensitive, unstable, and easy to shrink and crack. Laterite is a special clay formed with kaolinite as the main clay mineral [4, 5]. Iron oxide colloids in laterite play the key role in internal cementation [6–8]. The understanding of colloids in laterite is crucial for the insight of the formation process and mechanical characteristics of the laterite. The impact of the cementing effect of iron on the mechanical characteristics of the laterite has been investigated by existing studies. Some studies indicated that the mechanical properties of laterite can be improved to a certain level by increasing iron oxide colloid in the soil [9, 10]. Moreover, adding iron oxide colloid into kaolin sample can improve the surface area, pore ratio and other physical properties of the sample [11]. Moreover, the anti-shear strength and plastic limit of the soil sample and other indicators were improved [12]. It means that the content of iron oxide colloid would impact the physical properties of kaolin soil. In order to investigate the impact of cementing substances of soil, Cheng compared the original soil samples of the residual soil of Xiamen granite with the samples without the cementing substances. The result shows that the free iron oxide has significant

*Author to whom correspondence should be addressed.

Materials Express

impact on the expansibility and shear strength of soil samples [13]. In Ref. [14], author proved the cementing effect of free iron oxide in clay by showing that the porosity ratio and internal friction angle of clay decreased when iron are removed.

The reliability and accuracy of the preparation method of iron oxide colloid is very crucial for investigating the impact of colloids on the mechanical properties of soils. Via the centrifugal method, Bradfield added ammonium hydroxide to a concentrated iron chloride solution to prepare iron hydroxide colloids in the new sediment [15]. Chaudhury cemented newly precipitated iron hydroxide with an iron chloride solution, and performed dialysis for the soil [16]. Vora added a potassium cyanide solution to a zinc sulfate solution to obtain a colloidal solution [17]. Then, Vora filtrated the solution through a double-layer filter paper and used the parchment bag for dialysis [17]. The electrodialysis technology is also applied to purify the colloids. Recently, Chen proposed the colloidal titration method to determine the colloidal concentration [18]. Numbers of methods are proposed to prepare, purify, and determine of colloids in literature. However, the existing methods of colloid-related research still have limitations, such as low efficiency and low accuracy in sample preparation. In order to overcome the limitations, a set of rapid colloidal preparation equipment is developed in this paper. The device was verified according to the criteria proposed in Ref. [19].

The impact of free iron oxide on the geological properties and engineering performance of laterite has been mentioned by some studies. However, they did not provide in-depth knowledge. In this paper, by using kaolin the raw material of artificial clay, the impact of free iron oxide on the mechanical strength of laterite is systematically investigated. Moreover, the impact of artificial laterite preparation method on the macro-mechanical properties of soil samples is estimated. The forming mechanization of laterite is revealed by varying the mineral composition, microporousness and particle position in the sample. The major contribution of this paper is that the results provide deeper insight into the formation mechanism of laterite. Moreover, this paper uncovered why the characteristics of laterite vary with regions. It provides the theoretical support for the real-world engineering activity in laterite areas [20–28].

2. MATERIALS AND METHODS

2.1. Materials

Kaolin: H_2O, Fe $(NO_3)_3 \cdot 9H_2O$, NaOH.

Table I shows the chemical composition of kaolin. The chemical composition of the soil sample was measured by XRD test.om the top electrode to the bottom electrode, and was defined as negative when the current flowed in the opposite direction.

Table I. Chemical composition of kaolin.

Chemical element	SiO_2	Al_2O_3	Fe_2O_3	CaO	MgO	TiO_3	Na_2O+K_2O
Content (%)	54.41	39.19	0.18	0.35	0.25	0.8	1.2

Test soil sample: The prepared Fe $(OH)_3$ colloid was mixed into kaolin clay at a ratio of 24 wt.% In order to prepare the soil samples with a certain dry density, the solidification time of the soil sample was set to 7 days.

2.2. Development of Colloid Preparation and Test Equipment

Figure 1 shows the proposed device for rapid preparation of iron hydroxide colloid. The performance of the device is verified in Section 2.1. In order to filter out iron ions, chloride ions and other impurities in the colloid, the prepared colloid was filtered through a semi-permeable membrane. Generally, existing devices needs approximately 6 hours to prepare 1 liter iron hydroxide colloid. However, the proposed device is able to prepare colloid continuously, which produce 2 liter colloid per hour (see Fig. 1(A)). The circulation of deionized water is used to let most ions and other smaller substances passing through the semi-permeable membrane, while ensuring that the $Fe(OH)_3$ colloid left in the device (see Fig. 1(B)). Moreover, the proposed device can accurately determine the concentration of $Fe(OH)_3$ colloidal molecules since the method can identify the titration endpoint accurately (see Fig. 1(C)).

2.3. Sample Preparation

First, we put 1 L 5% $Fe(NO_3)_3 \cdot 9H_2O$ solution in a stirrer with 440 rpm. Then, 200 ml of 2.5 mol/L NaOH solution (100 g of NaOH was added to 1 L of distilled water) has been slowly dropped in to the stirrer when the temperature is about 28 °C to prepare a hydrogen iron oxide colloid. The 5% $Fe(NO_3)_3 \cdot 9H_2O$ solution is prepared by adding 50 g $Fe(NO_3)_3 \cdot 9H_2O$ into 1 L distilled water. Moreover, 2.5 mol/L NaOH solution is prepared by adding 100 g NaOH into 1 L distilled water. Then, the prepared $Fe(OH)_3$ colloid is mixed into chemically pure kaolin according to different mass percentage. Afterward, the artificial clay samples are crystallized in oven at 60 °C, for 48 hours. During the crystallization process, the samples were continuously stirred. Finally, the crystallized soil samples were ground and sieved to prepare artificial clay samples with a certain dry density. The artificial clay samples were placed in a humidified tank for curing group.

2.4. Test Plan

2.4.1. Unconfined Compressive Strength (UCS) Test

Because of the simplicity and reliability, the UCS test adopted to examine the sensitivity of laterite. The sensitivity reflects the structural strength of the soil, the changes

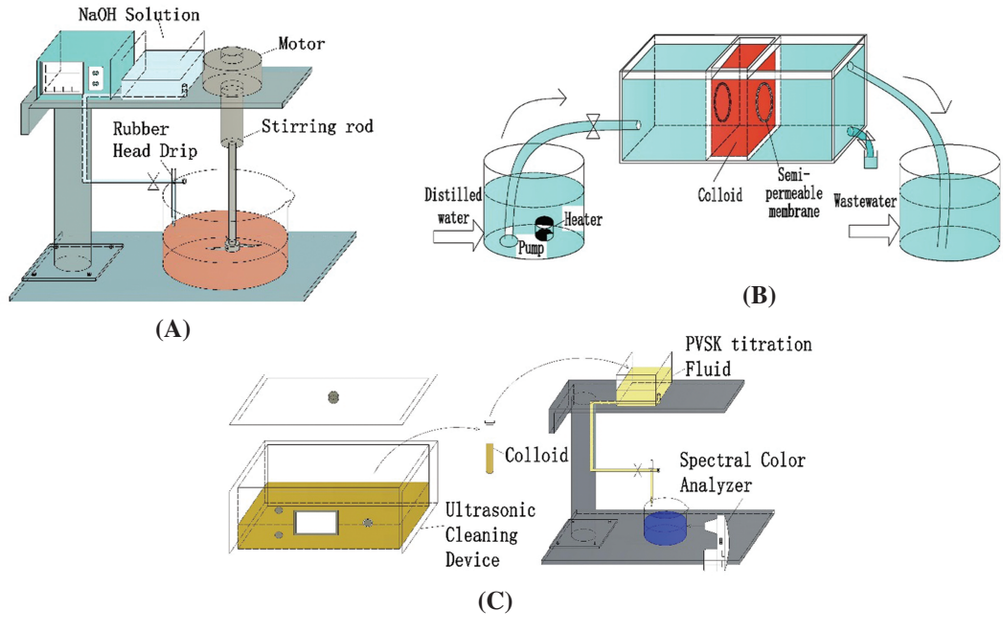

Fig. 1. Colloid preparation device. (A) Rapid colloid preparation device (B) Semipermeable membrane rapid dialysis device (C) Schematic diagram of the device for determining colloidal concentration for developing a device.

of the particle framework, and cementation strength during the laterization.

The artificial laterite samples, which are prepared for unconfined compressive strength test, contained 24 wt.% free iron oxide. Moreover, to explore the structural changes in the laterite process, the curing times of artificial laterite samples were set to be 7, 14, and 28 days, separately. The UCS test terminated with the axial strain $\varepsilon = 20\%$. The test equipment used YYW-II strain-controlled unconfined pressure gauge (China), and the pressure test rate was 0.1 mm/min.

2.4.2. Microscopic Test

The microscopic tests, which include X-ray diffraction, electron scanning test, and nuclear magnetic resonance test, are applied to measure the change of minerals, morphological characteristics, and micropores during lateritization. Among them, X-ray diffraction measures the mineral composition of soil samples and the changes of iron oxide minerals during the lateritization process. Electronic scanning test measures the morphological changes of kaolinite and iron oxide minerals. Nuclear magnetic resonance (NMR) test determine kaolinite and oxidation Characteristics of micro-pores of iron minerals during lateritization.

The container, which holds the sample for NMR test, should not contain any magnetic materials. At the same time, since the nuclear magnetic resonance instrument used in this paper measured 1 H, the container must not have hydrogen atoms. Consequently, the container is made by polytetrafluoroethylene since it has excellent chemical durability, decay resistance, acid-base resistance property, no static effect, and low friction coefficient. The size of this container is $\varphi = 39.1$ mm $\times$ H $= 80$ mm.

X-ray diffractometer D/max 2500 (scanning range 2°–90°), ΣIGMA scanning electron microscope (Karl Zeiss Microscope Co., Ltd., UK) and MacroMR12-150H-1 large-caliber nuclear magnetic resonance instrument (Suzhou Newmai Corporation) are applied to measure samples separately. The diameter of the coil in the NMR test was 60 mm.

3. RESULTS AND DISCUSSION

3.1. Compressive Strength

Figure 3 shows the compressive strength changing pattern of the original and remodeled samples of 24 wt.% laterite with different curing time. In this paper, the objective of the UCS test is to investigate the effect of free iron oxide on the formation of laterite soil structure.

As shown in Figure 2, the laterite samples did not have any damage or change during the curing process. It means that the free iron oxide can improve the compressive strength of the laterite. The increase in strength depends on the curing time of the free iron oxide because of the cementing reaction of the free iron oxide reaction. With the increase of the axial strain, the axial stress of the original sample suddenly decreased to show a "collapse" feature. The peak of the reshaped soil samples lag behind the original soil sample. Moreover, the strength curve of the reshaped soil samples showed a continuous hardening feature. Unlike the sample of the original laterite, the peak strength of the reshaped samples are significantly

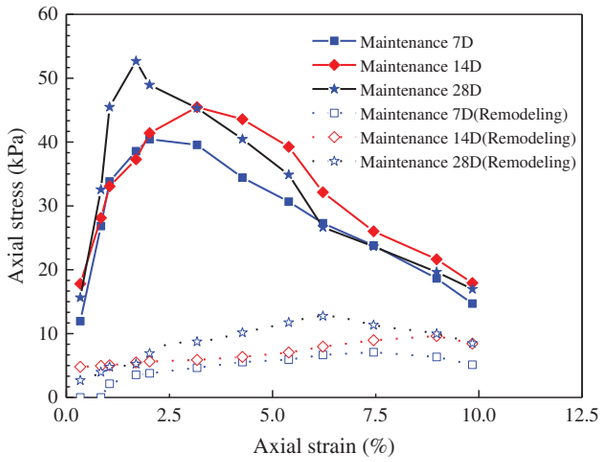

Fig. 2. Unconfined compressive strength test results of the specimens.

lower than the original samples. The major reason is that there constructed samples destroyed the structure of the soil body. Therefore, the connection between the soil particles disappears, which makes the structural strength of soil body decreases. In summary, the reason of lower strength of the remodeled samples could be caused by the failure of the soil sample structure and the change in the bonding strength of the free iron oxide [31–35].

When the curing time of the original soil sample reaches 28 days, the compressive strength of the artificial clay sample reached 53 kPa, and the strength increased by 3 kPa. Simultaneously, the non-lateral compressive strength of the reconstructed sample phase was significantly reduced for the original sample.

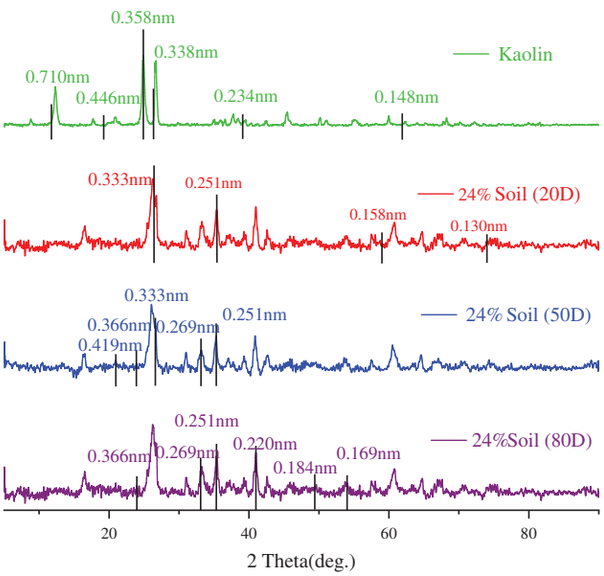

Fig. 3. Results of X-ray diffraction study of different soil samples.

The sensitivity of soil samples were determined from the results of the UCS test and the values were compared with the sensitivity of the artificial clay samples of Cheng. The test results are listed in Table II.

As seen from Table II, the growth pattern of the non-lateral compressive strength of artificial clay samples agrees with the actual situation. Considering identical curing conditions, only free iron oxide colloids affect the lateral compressive strength of soil. The reasons for the intensity differences under identical curing condition and iron content are related to the purity of the iron hydroxide colloid.

The structure of soil is determined by the combination of soil particles and the coupling characteristics of soil particles. In the equilibrium state, iron oxide colloid and water are present between soil particles. The partial binding water between soil particles is converted into free water when the soil is under an external load, resulting in the reduction of the compressive and shear strength of the soil. The strength of laterite is mainly caused by the adhesion between particles and the adhesion force formed by iron oxide colloid. When the soil is disturbed, these two types of adhesion are destroyed or partially destroyed, and the soil strength decreases [36, 37].

Microscopic structure analysis showed that the test soil sample was composed of countless small soil particles, and these soil particles on the surface of negative electricity. When the free iron oxide content in the soil increases, according to the Coulomb's law for the free iron oxide with positively charged iron ions, the ions will be adsorbed on to the surface of the negatively charged soil particles. Hence, the radius of soil particles increases. In the same way, the positive charge on the surface of soil particles will attract other soil particles with negative charges on their surface. Hence, soil particles gather together, strengthening the attraction between soil particles. Meanwhile, the condensate in the increasing soil, promoting the bonding effect to increase the overall strength of the soil. Therefore, the non-lateral compressive strength of soil samples with high iron content is larger.

Table II. Test results of unconfined compressive strength and sensitivity.

Soil sample	Number of days of maintenance (D)	Unconfined compressive strength test (kPa)	Sensitivity
Kaolin	7	20	–
	14	20	–
	28	20	–
Artificial clay sample (Cheng [40])	7	41	2
	14	37	2
	28	45	2
Artificial clay sample (This paper)	7	40.4	5.7
	14	45.5	4.7
	28	52.7	4.3

Article

Soil sensitivity reflects the degree of change in the intensity of soil due to structural damage, and it is an important reference index for laterite with distinct properties. The data in Table II show that the sensitivity of artificial clay samples changed with increase in maintenance time, increasing to 5.7. The sensitivity was 4.3 after 28 days of maintenance. The structural changes in the soil show that cementation plays an important role, and the large pore structure inside the soil gradually develops in the direction of small pores, thereby enhancing the structure of the soil. This process of change can reflect the historical process of the clay formation to a certain extent.

The structural connection in clay is mainly an iron-cemented connection, and the strength of the link is related to the shape of the free iron oxide, and the cementing connection strength of the needle-shaped iron ore and hematite is greater than that of the gel state. The oxygen atom on the surface of kaolin combines with Fe gel under certain curing conditions to form a homogeneous aggregate of silicone oxygen tetrahedrons, and this effect will evolve into a "homologous" connection between particles. This connection between clay particles and Fe gel is quite solid because of the increasing structural connection strength of artificial clay samples with increasing curing time. Meanwhile, the stiffness of soil structures is increased by the same contact of silica, and hence, brittle failure is observed to occur in the test of compressive strength without lateral limits.

In summary, the intensity change process of laterite can be specifically expressed as follows: First, the free iron oxide in the soil skeleton and kaolin form an agglomerate by bonding, part of the free iron oxide cement fills the pores, and the other part of the free iron oxide cements. The material is wrapped around the edge of the kaolin aggregate. This bonding is formed by cementation; then, the morphology of the free iron oxide changes to form goethite and hematite, the cementation strength of the free iron oxide mineral is enhanced, and the kaolin particles and free iron oxide form a silicon-oxygen tetrahedron "Homogeneous hyperplasia" increases the stiffness of the soil structure. Therefore, with the increasing time of laterization or the formation of the soil particle skeleton, the mechanical strength of the laterite increases.

3.2. X-ray Diffraction (XRD) Contrast Test

Figure 3 shows soil samples with kaolin clay and free iron oxide content of 24 wt.% In a humidifier for 20, 50, and 80 days. The characteristic XRD peaks of kaolin are d(001) = 0.715 nm, d(002) = 0.357 nm, and d(002) = 0.337 nm [21–23]. The XRD intensity of kaolin corresponding to the characteristic peak increases, indicating that the relative content of kaolin increases, and conversely, the relative content of kaolin decreases. The analysis results show that kaolin is mainly composed of kaolinite minerals and a small amount of feldspar and quartz minerals.

The XRD spectrum shows two major differences upon the addition of iron hydroxide colloid to kaolin: First, the peak shifts from 0.71 nm to 0.333 nm, indicating that the crystal structure of kaolinite has changed. Second, with an increase in maintenance time, the main variation range of the XRD spectrum is 20°–60°; changes in this range of angle are mainly due to the formation of minerals such as needle-shaped iron ore and hematite, which in turn reflects the change in the mineral composition of soil. The characteristic XRD peaks of needle-shaped iron ore are 21.2°, 333.2°, 40.94°, and 49.54° at 50 days during the maintenance of the artificial clay samples. For a curing time of 80 days, the characteristic XRD peaks of hematite and needle iron ore appear at 21.1°, 24.3°, 33.2°, 34.85°, 36.8°, 40.94°, and 49.59°, which shows that the morphology of free iron oxide in artificial clay samples increases with time. The form of iron underwent a transformation from pyrite → pyrite → pyrite → hematite [24, 25]. Meanwhile, the capsule formed by free iron oxide shielded the sharp peaks of kaolin. Therefore, a low and smooth diffraction peak of the artificial clay sample was obtained.

From the XRD images, we can conclude that the longer the curing time of the laterite-like sample, the different the free iron oxide minerals in the reaction products changed. At the same time, different free iron oxide minerals can reverse the laterite process of laterite.

3.3. Scanning Electron Microscope Test

Figure 4 is a SEM image of 24 wt.% Laterite. The SEM images show that the artificial clay sample is composed of irregular unit aggregations of different sizes, with a relatively clear boundary line between the units. Figure 4(a) shows an SEM image of 24 wt.% free-iron-oxide-mixed sample with 56 days of maintenance. In the picture, the red dotted lines represent the shape of kaolin particles. The green dotted line indicates the contour and position of the free iron oxide. The clay particles have free iron oxide on the surface or granular agglomerates. According to the test results, it is shown that with the increasing time of laterization, due to the action of free iron oxide, the bonding mode of the unit cells in the soil has changed, and this change has caused changes in the macro-mechanical nature of the soil. The soil body was assumed as follows: free iron oxide and kaolin having the same layered structure as the lamella keep its shape almost unchanged, and the SEM image in Figure 4(b) is a laterite sample formed by cementation or lateration.

3.4. Nuclear Magnetic Resonance Test

Figure 5 is the T2 curve of 24 wt.% Laterite samples at different curing times. Due to the existence of isolated pores inside the aggregate formed by the free iron oxide cement, this caused the phenomenon of "doublet" or "multimodal" in the NMR T2 curve. Under the same curing time and dry density conditions, with the increase of free iron oxide

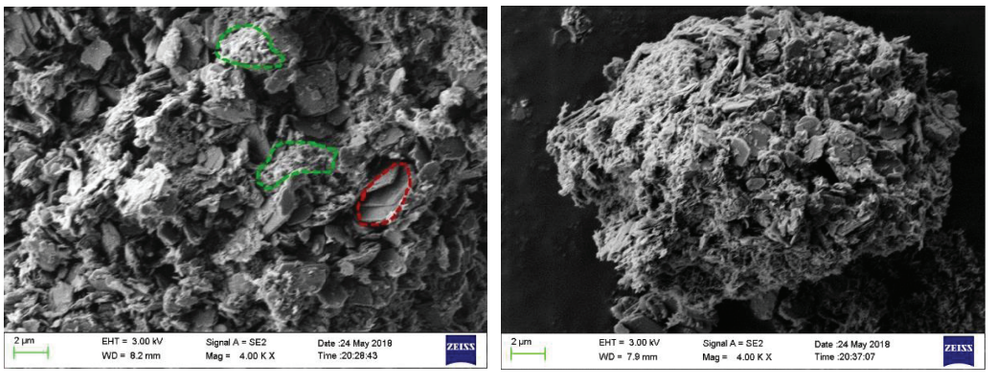

(a) (b)

Fig. 4. Scanning electron microscopy images of laterite.

cement, more laterite particle gaps and inner pores of the formed aggregates will be filled by these gel particles, and gradually form more "Sturdy" skeleton. This causes the reduction of the number of pores in laterite samples with high cement content. The T2 curve distribution of the laterite sample shows three peaks. The first relaxation peak is mainly distributed between 0.01 ms and 0.13 ms, the second relaxation peak is mainly distributed between 0.42 ms and 18 ms, and the third relaxation peak is distributed. Between 25.5 ms–205 ms. The first relaxation peak has an increasing trend, indicating that the size of the pores is decreasing, and the number of pores is also increasing; aggregates formed by the cementation of the cement and kaolin fill the large pores, and A part of the cement fills the intercrystalline pores between the soil particles. This caused the T2 distribution curve to shift to the left.

3.5. Laterite Particle Contact Model

The development process of the non-lateral compressive strength curve of the specimen can be divided into three stages: initial stage (6a, 6b), ascending stage (6c), and softening stage (6d) [38, 39]. In the initial stage of the specimen, a small amount of free iron oxide cementation is distributed around kaolin. As shown in Figure 6, as the strain increases, the connection of clay particles and cementation change in two different ways: one is the reduction of the pores of the overhead structure between the soil particles, and displacement of the particles, which increases the friction between the particles in the soil sample, thereby increasing the axial stress to reach a relatively high level (Fig. 6(C)). As the strain increases further, the connection between the particles is destroyed, and the structural units between the soil particles are completely destroyed, as shown in Figure 6(D).

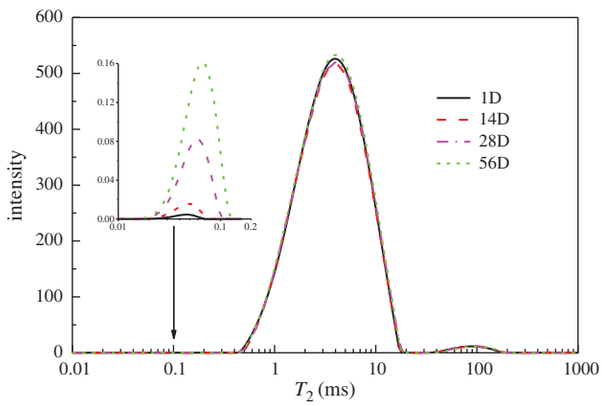

Fig. 5. T_2 distribution of 24 wt.% laterite soils.

Based on the SEM results, an abstract particle contact model was established. The model was used to explain the results of sample strength changes with increasing curing time. The model showed changes in the relative position of soil particles during loading.

The sample in Figure 6(A) is a triaxial sample of pure kaolin, and Figures 6(B)–(D) are 3D schematic diagrams of the saturated sample of 24 wt.% triaxial laterite from the beginning of loading to failure. Figure 6(a) shows the formation of smaller aggregates by filling or cementing the colloids in the soil particles, and Figures 6(b)–(d) show the destruction of the structural unit body between the soil particles.

With the increase of strain in the laterite sample, there are two changes in the connection between clay particles and cement. One is that the pores in the overhead structure between the soil particles are reduced, and the position of the particles is shifted, which increases the particles in the soil sample. Therefore, the axial stress can reach a relatively high level. As the strain further increases, the connection between the particles is broken, and the structural unit body between the soil particles is completely destroyed.

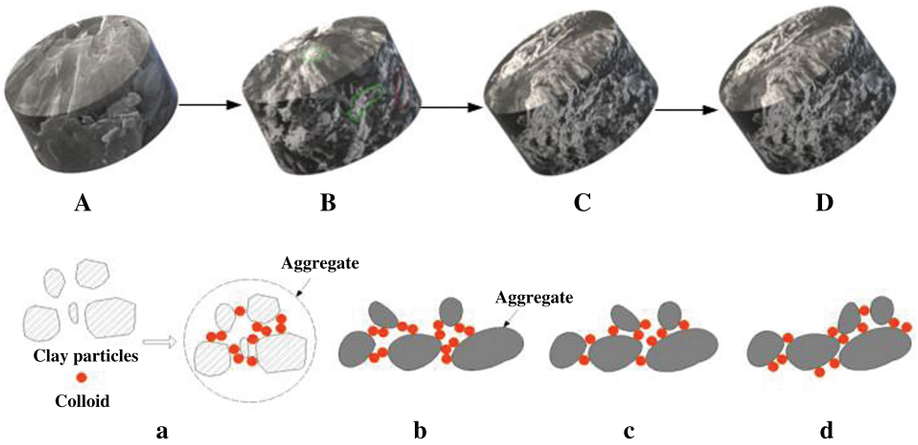

Fig. 6. Schematic diagram of the microscopic structure contact model of laterite.

4. CONCLUSIONS

A tested rapid colloid preparation device was used to prepare iron hydrogen colloid. The laterite which is formed by agglomeration of free iron oxide and kaolin is used to carry on the strength experiment and related micro experiments. The experimental results of this study show that during the dynamic cementation process of free iron oxide from ionic state to crystalline, laterite is a kind of soil that the basic unit body changes from the gel state of sheet aerial structure to the microcrystalline state of a dense granular structure. In the soil samples with crystalline development, the strength of laterite gradually increases with the process of laterization, which causes the difference in strength of laterite to a large extent depends on the content of free iron oxide, the type of free iron oxide minerals, and the microstructure inside the soil. With the increase of curing time of laterite, the laterization is enhanced with the increase of the cohesive force, friction angle and the number of micro pores. The cement is mainly distributed in the clay particles According to the scanning electron microscopy (SEM) image display results, an abstract particle contact model was established in the surface of the surface or the pores between clay particles, which can fully reflect the free cemented iron oxide, which is the main cementing material, in the process of stress on laterite. Role in laterite. This study can improve the understanding of the relationship between macro-mechanical properties and micro-factors of laterite under natural conditions. So it provides a new idea for the study of the engineering properties of such regional special soils. It has very important and positive guiding significance for reducing the blindness in engineering and the practice of laterite engineering.

Conflicts of Interest

The authors declare no conflicts of interest.

Acknowledgments: This work was funded by the Guangxi Zhuang Autonomous Region Natural Science Foundation of China (No. 2018GXNSFDA281038) and Guangxi Key Laboratory of Geomechanics and Geotechnical Engineering of China [No. 13-KF-05].

References and Notes

1. Persons, B.S and Fairbridge, R.W., **1972**. Laterite: Genesis, location, use. *Soil Science*, *113*(4), pp.302–303.
2. Zhang, J.-K., Dong, H., Cheng, Y.-P., Yue, C. and Liu, K., **2020**. Compilation of hydrogeological map of China. *Journal of Groundwater Science and Engineering*, *31*(4), pp.80–94.
3. Ghosh, S., Guchhait, S.K., Illahi, R.A., Bera, S., and Roy, S., **2021**. Geomorphic character and dynamics of gully morphology, erosion and management in laterite Terrain: Few observations from Dwarka-Brahmani Interfluve, Eastern India. *Geology Ecology and Landscapes*. DOI: 10.1080/24749508.2020.1812148.
4. Madu, R.M., **1997**. An investigation into the geotechnical and engineering properties of some laterite of Eastern Nigeria. *Engineering Geology*, *11*, pp.101–125.
5. Jenny, H., **1994**. Factors of soil formation: A system of quantitative pedology. *Geoderma*, *68*(2), pp.335–336.
6. Thomas, M.F. and McFarlane, M.J., **1979**. Laterite and landscape. *Geofisica International, Africa*, *49*(1), pp.89–90.
7. Saeed, Z.K. and Berenjian, A., **2013**. Soil formation by ecological factors: Critical review. *American Journal of Agricultural and Biological Science*, *8*(2), pp.214–216.
8. Wang, Y. and Gao, Z.J., **2016**. Discussion on the research progress of clay. *Technology Innovation and Application*, *6*(21), pp.182–183.
9. Hu, G.C., Zhang, M.K. and Han, C.C., **2000**. Preliminary study on mechanics and acid-alkali stability of red soil agglomerates. *Journal of Zhejiang Agricultural Science*, *3*, pp.125–127.
10. Hu, G.C. and Zhang, M.K., **2002**. Mineralogical proof of strong cementing effect of free iron oxide on soil particles. *Chinese Journal of Soil Science*, *33*(1), pp.25–27.
11. Luo, H.X., **1983**. Effects of amorphous substances on the mechanical properties and structure of soil. *Rock and Soil Mechanics*, *4*(1), pp.67–72.
12. Feng, J.L., Zhao, Z.S. and Gao, G.R., **1994**. Study on the function and mechanism of free iron oxide in laterite. *Journal of the Hebei Academy of Sciences*, *4*(1), pp.35–43.
13. Cheng, C.B. and Xing, C.W., **1986**. Cementation characteristics of granite residues and their effects on mechanical properties. *Rock and Soil Mechanics*, *7*(2), pp.61–66.

Article

14. Wang, J.Z., **1983**. Effects of free iron oxide on engineering characteristics of laterite. *Chinese Journal of Geotechnical Engineering*, *5*(2), pp.147–156.
15. Bradfield, R., **1922**. A centrifugal method for preparing colloidal iron hydroxide, aluminum hydroxide and silicic acid. *Journal of the American Chemical Society*, *44*(5), pp.965–974.
16. Chaudhury, S.G. and Ganguli, A., **1927**. The effect of non-electrolytes on the stability of colloids II: Ferric hydroxide sol. *The Journal of Physical Chemistry*, *32*(12), pp.1872–1874.
17. Vora, V.C., Barve, P.M. and Desai, B.N., **1941**. Importance of dialysis in the study of colloids. *Proceedings of the Indian Academy of Sciences-Section A*, *13*(2), pp.100–107.
18. Chen, B.Q., Bai, Y.W., Wang, Y.Q. and Li, W.J., **1983**. Study on colloidal titration and its standard reagents. *Journal of Taiyuan University of Technology*, *12*(3), pp.85–92.
19. Rozos, D. and Koukis, G., **1986**. An investigation of the mineralogical, physical and mechanical properties of Greek laterites. *Bulletin of Engineering Geology and the Environment*, *33*(1), pp.91–96.
20. Yang, D.L., **2004**. Study on the causes and effects on engineering of red clay in Southern Anhui. *Geology of Anhui*, *1*(04), pp.304–307 + 311.
21. David, J., Brown, P.A. and Helmke, M.K., **2003**. Clayton: Robust geochemical indices for redox and weathering on a granitic laterite landscape in central Uganda. *Geochimica et Cosmochimica Acta*, *67*(15), pp.2711–2723.
22. Coussy, S., Grangeon, S., Bataillard, P., Khodja, H., Maubec, N. and Faure, P., **2017**. Evolution of iron minerals in a 100 years-old technosol: Consequences on Zn mobility. *Geoderma*, *290*, pp.19–32.
23. Verboom, W.H. and Pate, J.S., **2003**. Relationships between cluster root-bearing taxa and laterite across landscapes in southwest Western Australia: An approach using airborne radiometric and digital elevation models. *Plant and Soil*, *248*(1–2), pp.321–333.
24. Costa, M.L.D. and Leite, A.S., **2016**. A laterite-hosted APS deposit in the amazon region, Brazil: The physical-chemical regime and environment of formation. *Journal of Geochemical Exploration*, *170*, pp.107–124.
25. Cherdsak, S., Niti, T. and Jaksada, T., **2019**. Compressive strength of marginal lateritic soil stabilized. *International Journal of Engineering and Technology*, *11*(3), pp.177–180.
26. Muhiddin, A.B. and Tangkeallo, M.M., **2020**. Correlation of unconfined compressive strength and california bearing ratio in laterite soil stabilization using varied zeolite content activated by waterglass. *Materials Science Forum*, *998*(1), pp.323–328.
27. Wang, J., Dong, S., Zhou, C., Ashour, A. and Han, B., **2021**. Investigating pore structure of nano-engineered concrete with low-field nuclear magnetic resonance. *Journal of Materials Science*, *56*(1), pp.243–259.
28. Ahmad, B., Abdurrahman, Y. and Murtala, U., **2021**. Assessment of lateritic soil stabilized using metakaolin. *Journal of Geotechnical Studies*, *5*(1), pp.15–26.
29. Verboom, W.H. and Pate, J.S., **2003**. Relationships between cluster root-bearing taxa and laterite across landscapes in southwest Western Australia: An approach using airborne radiometric and digital elevation models. *Plant and Soil*, *248*(1–2), pp.321–333.
30. Costa, M.L.D. and Leite, A.S., **2016**. A laterite-hosted APS deposit in the amazon region, Brazil: The physical-chemical regime and environment of formation. *Journal of Geochemical Exploration*, *170*, pp.107–124.
31. Lohr, S.C. and Murphy, D.T., **2017**. Maghemite soil nodules reveal the impact of fire on mineralogical and geochemical differentiation at the earth's surface. *Geochimica Et Cosmochimica Acta*, *200*, pp.25–41.
32. Das, D. and Kar, B.B., **2020**. Impact of soil moisture and soil temperature on the physico-chemical property of laterite soil. *Asia Journal of Water. Environment and Pollution*, *17*(1), pp.91–96.
33. Al-Mukhtar, M., Khattab, S. and Alcover, J.-F., **2012**. Microstructure and geotechnical properties of lime-treated expansive clayey soil. *Journal of Engineering Geology*, *139–140*, pp.17–27.
34. Pakbaz, M.S. and Mohsen, F., **2015**. Comparison of the effect of mixing methods (dry vs. wet) on mechanical and hydraulic properties of treated soil with cement or lime. *Applied Clay Science*, *105*(3), pp.156–169.
35. Marta, D.S., Evelina, F. and Francesco, M., **2014**. Time of reactions in a lime treated clayey soil and influence of curing conditions on its microstructure and behaviour. *Applied Clay Science*, *99*, pp.100–109.
36. Makki, S.L., Hibouche, A., Taibi, S., Gontran, H.C., Didier, L.C. and Jean, M.F., **2015**. Evolution of the properties of lime-treated silty soil in a small experimental embankment. *Journal of Engineering Geology*, *191*, pp.8–22.
37. Jha, A.K. and Sivapullaiah, P.V., **2016**. Volume change behavior of lime treated gypseous soil influence of mineralogy and microstructure. *Applied Clay Science*, *119*, pp.202–212.
38. Lu, R.N. and Gong, T.Z., **2016**. Method for determination of sensitivity of primary ground saturated silt in Fenhe river. *Journal of Electric Power*, *31*(3), pp.251–258.
39. Rizvi, Z.H., Nikoli, M. and Wuttke, F., **2019**. Lattice element method for simulations of failure in bio-cemented sands. *Granular Matter*, *21*(2), pp.1–14.
40. Cheng, C.B. and Tang, Z.L., **1992**. A preliminary study on the nature of "cementation" between goethite and kaolin. *Rock and Soil Mechanics, 13*(2), pp.122–127.

Received: 27 November 2020. Accepted: 15 February 2021.

Article